Cell Reports

Article

Prefrontal cortex neuronal ensembles dynamically encode task features during associative memory and virtual navigation

Graphical abstract

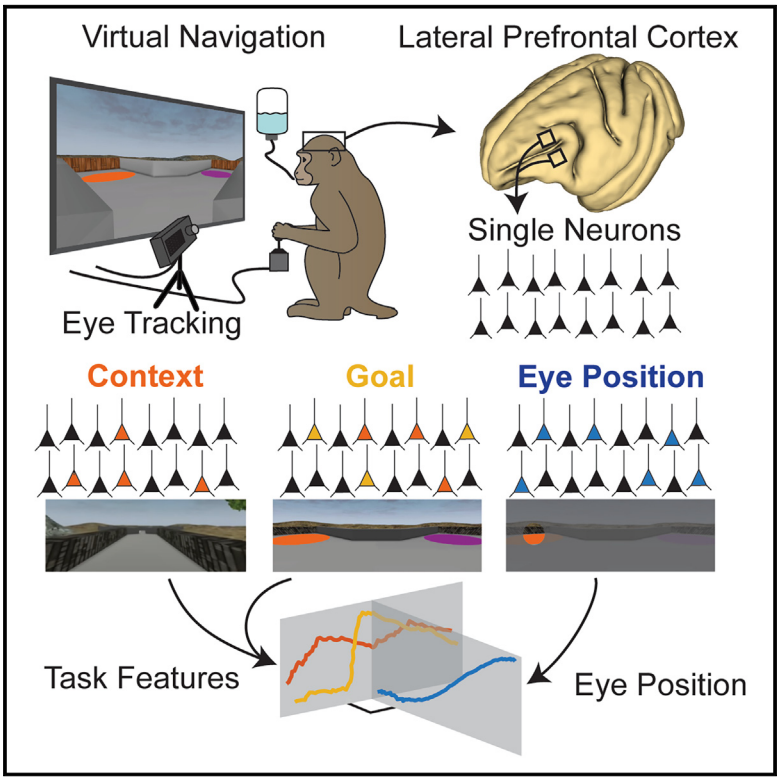

Authors

Mohamad Abbass, Benjamin Corrigan, Renée Johnston, Roberto Gulli, Adam Sachs, Jonathan C. Lau, Julio Martinez-Trujillo

Correspondence

julio.martinez@robarts.ca

In brief

Abbass et al. demonstrate that neurons in the lateral prefrontal cortex of non-human primates dynamically mix eye position and visual task features during virtual navigation. Neurons located dorsally preferentially represent spatial features, while ventral neurons represent visual features in a different subspace than eye position.

Highlights

- Lateral prefrontal cortex neurons are tuned to visuospatial features during navigation
- Neurons dynamically mix unconstrained eye position and visual features
- Dorsal and ventral neurons represent spatial and visual features, respectively
- Eye position is represented in a different subspace than visual features

Abbass et al., 2025, Cell Reports *44*, 115124
January 28, 2025 Crown Copyright © 2024 Published by Elsevier Inc.
https://doi.org/10.1016/j.celrep.2024.115124

CellPress

Cell Reports

CellPress
OPEN ACCESS

Article

Prefrontal cortex neuronal ensembles dynamically encode task features during associative memory and virtual navigation

Mohamad Abbass,[1,2] Benjamin Corrigan,[2,3] Renée Johnston,[4,5] Roberto Gulli,[6,7] Adam Sachs,[4,8] Jonathan C. Lau,[1,2] and Julio Martinez-Trujillo[1,2,3,9,*]

[1]Western Institute for Neuroscience, Western University, London, ON, Canada
[2]Department of Clinical Neurological Sciences, London Health Sciences Centre, Western University, London, ON, Canada
[3]Department of Physiology and Pharmacology, Schulich School of Medicine and Dentistry, Western University, London, ON, Canada
[4]Ottawa Hospital Research Institute, Ottawa, ON, Canada
[5]University of Ottawa Brain and Mind Research Institute, Ottawa, ON, Canada
[6]Zuckerman Mind Brain Behavior Institute, Columbia University, New York, NY, USA
[7]Center for Theoretical Neuroscience, Columbia University, New York, NY, USA
[8]Division of Neurosurgery, Ottawa Hospital Research Institute, Ottawa, ON, Canada
[9]Lead contact
*Correspondence: julio.martinez@robarts.ca
https://doi.org/10.1016/j.celrep.2024.115124

SUMMARY

Neuronal populations expand their information-encoding capacity using mixed selective neurons. This is particularly prominent in association areas such as the lateral prefrontal cortex (LPFC), which integrate information from multiple sensory systems. However, during conditions that approximate natural behaviors, it is unclear how LPFC neuronal ensembles process space- and time-varying information about task features. Here, we show that, during a virtual reality task with naturalistic elements that requires associative memory, individual neurons and neuronal ensembles in the primate LPFC dynamically mix unconstrained features of the task, such as eye movements, with task-related visual features. Neurons in dorsal regions show more selectivity for space and eye movements, while ventral regions show more selectivity for visual features, representing them in a separate subspace. In summary, LPFC neurons exhibit dynamic and mixed selectivity for unconstrained and constrained task elements, and neural ensembles can separate task features in different subspaces.

INTRODUCTION

The primate lateral prefrontal cortex (LPFC) sits on top of the sensorimotor processing hierarchy and has been implicated in cognitive functions, including selective attention, working memory, and rule encoding.[1–3] Single neurons in the LPFC have been reported to be tuned to multiple task features in visuomotor tasks.[4–6] This property has been termed "mixed selectivity," where neural responses to a combination of variables can be combined either linearly or nonlinearly.[7] Non-linear mixed selectivity has been suggested to be behaviorally and computationally relevant, as it can increase the dimensionality of representations and facilitate readouts of task-relevant features.[7,8] However, most tasks exploring selectivity in LPFC neurons have been conducted using simple visual displays and constraining eye movements. It remains unclear how individual neurons and neuronal ensembles in the LPFC mix information in scenarios with complex dynamic scenery, unconstrained eye movements, and sensorimotor events occurring in a continuous and dynamic manner.

The LPFC is heavily interconnected with numerous cortical areas and has been cytoarchitecturally divided into areas 8, 9, 10, 12, 45, and 46v/d, with tracing studies describing distinct anatomical connectivity patterns across these areas.[1,9,10] A recent study revealed distinct functional connectivity patterns in the dorsal (e.g., areas 9/46) and ventral (areas 45/47) LPFC, corresponding to dorsal and ventral high-level sensory areas, respectively.[11] However, a functional organization of the LPFC has not been delineated as clearly. Single neurons in the dorsal and ventral LPFC have been reported to preferentially represent spatial and visual/object information, respectively.[12–14] However, representations of numerous modalities and levels of sensory integration have been reported in both the dorsal and ventral LPFC.[15–17] These findings may be linked to the integrative nature of the LPFC, with its ability to merge task-relevant information.[2,3]

Previous studies have shown that neurons in the LPFC can become selective for combinations of relevant features during associative learning tasks.[4,5,18] However, these studies have used behavioral tasks involving controlled stimulus presentation of few task-relevant features in simple displays while

 Crown Copyright © 2024 Published by Elsevier Inc. This is an open access article under the CC BY license (http://creativecommons.org/licenses/by/4.0/).

constraining eye movements. The LPFC must be able to perform its function under real-world conditions, while subjects perform complex tasks and explore visual scenes via gaze shifts. Tremblay et al.[19] demonstrated that single neurons in the LPFC maintain their representation of task features during unrestrained gaze movements. Moreover, Roussy et al.[20] showed that representations of spatial locations by many LPFC neurons during virtual reality navigation in complex visual environments remain robust to changes in gaze position. These studies suggest that many LPFC neurons contain spatiotopic representations of the environment. More recently, Corrigan et al.[21] have shown that LPFC neurons encode views of visual scenes, suggesting that LPFC neurons may mix spatial and non-spatial information. However, it is unclear whether these components of mixed selectivity multiplex over time or are mixed together in a single multidimensional representation.

Here, we investigate how mixed selective neurons in the LPFC (areas 9/46) encode spatial and non-spatial features of the environment during an associative memory task that requires virtual navigation through a complex visual environment. To this end, we recorded the responses of hundreds of neurons in two monkeys (*Macaca mulatta*) as they completed the task and freely explored the different elements of the visual scene via gaze shifts. Importantly, the task had different periods in which different features appeared serially. We found that individual neurons and neuronal ensembles in the LPFC mixed their representations of task-relevant features and space. The dorsal and ventral LPFC had different tuning profiles and temporal dynamics. The ventral LPFC preferentially represented non-spatial task features, whereas the dorsal LPFC predominantly encoded space.

RESULTS

We trained two male monkeys (*M. mulatta*) to perform a context-color association task in a virtual environment (Figure 1). The animals used a joystick to navigate in an X-shaped maze, with each trial beginning in one arm of the maze (Figure 1C). Once the monkeys entered the corridor, the walls changed texture to steel or wood (the context). When the monkeys reached the end of the corridor, two colored discs appeared, one at the end of each arm of the maze. The location of the colors (left or right arm) was determined randomly for each trial (color pair order [CPO]). The context determined the color disc to which the monkeys needed to navigate for a reward, termed ''target side'' (Figure 1D). Monkeys performed a fixed association trial block and then learned new associations each day. Performance varied from session to session but was significantly above the 50% chance level for most sessions (Figures 1E and S1C). Across all sessions, monkey B had a mean (±SE) of 80.9% ± 2.76% correct trials, and monkey T had a mean of 73.9% ± 5.43% correct trials. The naturalistic features of this task (e.g., gaze was unconstrained, and the animal initiated and conducted navigation at will using a joystick) allowed the monkeys to freely complete the task and navigate toward their goal with no additional behavioral constraints. Therefore, we measured the eye position and reaction time of joystick rotation, demonstrating that the monkeys fixated on their chosen side (Figures 1E and S1A).

LPFC neurons are modulated by eye position and task features

While the monkeys completed the virtual reality navigation task, we recorded from a total of 753 neurons (467 in monkey B and 286 in monkey T) during six sessions. Single neurons were isolated manually using spike sorting (STAR Methods). We computed firing rates and spike density functions for each isolated neuron and condition and found that many neurons gave distinctive responses between conditions (see the example in Figure 1F). Single-neuron tuning to task-related variables was determined using multivariable linear regression models (STAR Methods). Neurons exhibited minimal tuning to context after its appearance until shortly before goal onset (Figure S2A). Therefore, we focused on the goal onset epoch, where the monkeys must associate the context with the appropriate color and navigate toward it. This provided us with the opportunity to explore neural dynamics in the LPFC during real-world context-target associations. To this end, we investigated neural activity in the dorsal and ventral LPFC. The dorsal array covers regions of areas 8Ad and 46d. The ventral array covers the ventral subdivisions of these areas, 8Av and 46v, and may extend to area 45 (estimation according to Petrides[1]).

We first quantified the variance of single-neuron activity explained by the task features (Equation 3) and eye position (Equation 2). Overall, neural activity was dynamic and mixed, with many neurons being modulated by both eye position and task features (Figure 2A). Neurons in the LPFC were modulated by eye position more than by task features in both arrays and monkeys ($p < 0.001$, Wilcoxon rank-sum test; Figure 2B). Furthermore, neurons in the ventral LPFC were modulated by task features more than neurons in the dorsal LPFC in both monkeys, with a mean (±SE) R^2 of 0.114 ± 0.008 compared to 0.083 ± 0.004 in monkey B ($p < 0.01$, Wilcoxon rank-sum test) and a mean R^2 of 0.118 ± 0.066 compared to 0.096 ± 0.053 in monkey T ($p < 0.05$, Wilcoxon rank-sum test). Finally, many neurons showed mixed selectivity to eye position and task features (Figure 2C), demonstrating linear mixing (18% ventral, 17.2% dorsal in monkey B; 6.2% ventral in monkey T) and non-linear mixing (11.3% ventral, 12.1% dorsal in monkey B; 8.4% ventral, 8.9% dorsal in monkey T), and were tuned to those features at different times (11.3% ventral, 13.9% dorsal in monkey B; 16.3% ventral, 7.1% dorsal in monkey T). See Figure S2D for more details regarding each neuron's response to eye position and task features.

LPFC neurons mix task features

Using the same analysis as above, we further characterized neuron tuning to specific task features.

Because the target side was confounded by gaze, we report the proportion of neurons tuned to the side fixated on without removing eye position information (Equation 1). As expected, neuron tuning to task features changed over the course of the trial as information became available (Figure 3A; see Figure S2B for each session individually). Considering neurons tuned at any time around goal onset (−200 to 1,000 ms), monkey T had significantly different proportions of neurons tuned to task features between the ventral and dorsal LPFC. Specifically, more neurons in the ventral LPFC were tuned to context (39, 22.5%) compared to the dorsal LPFC (7, 6.2%; Fisher's exact test, $p < 0.001$). More

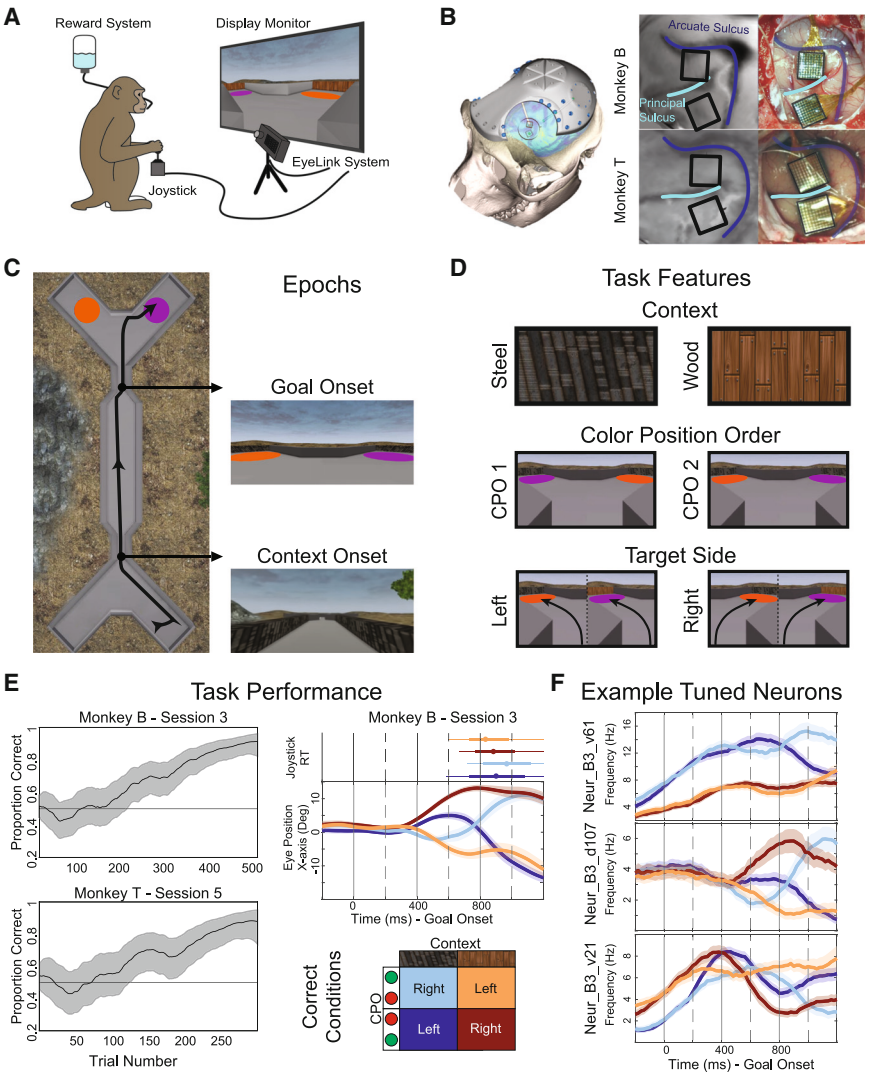

Figure 1. Recordings from non-human primate LPFC during a virtual navigation associative memory task

(A) Monkeys were seated in front of a monitor and used a joystick to navigate through the virtual reality maze to complete the associative memory task.

(B) Location of implanted Utah microelectrode arrays, placed in the dorsal (areas 9/46d) and ventral (area 9/46v) LPFC.

(C) Overview of the X maze, with an example path taken during one trial, with the onset of the context (walls changing to steel or wood) and goal (two possible colors per session appearing in a random order) indicated.

(D) All possible task conditions with context, color pair order (CPO), and target side.

(E) Estimated learning state in both monkeys with 95% confidence interval in example sessions with a novel context association. Shown is mean eye position on the x axis over 400-ms windows, demonstrating separation across conditions with fixation on the target side. Reaction time (RT), defined by rotating the joystick, is shown above for each condition (median circle, 25th–75th percentile thick line, 5th–95th percentile thin line).

(F) Mean firing rate over 400 ms in example neurons tuned to task features during goal onset, tuned to steel (above), eye position to the right (center), and mixed selectivity (bottom).

neurons were tuned to CPO in the ventral array (17, 9.8%) compared to the dorsal array (4, 3.5%), but this was not statistically significant using Fisher's exact test (p = 0.06). Finally, a similar proportion was tuned to the target side between the dorsal (18, 15.9%) and ventral LPFC (24, 13.9%; Fisher's exact test, p = 0.73). Monkey B, on the other hand, had a similar proportion of neurons tuned to context in the ventral (68, 35.1%) and dorsal LPFC (76, 27.8%; Fisher's exact test, p = 0.13) and CPO in the ventral (54, 27.8%) and dorsal LPFC (78, 28.6%; Fisher's exact test, p = 0.84). The target side was represented by more neurons in the dorsal (156, 57.1%) compared to ventral LPFC (91, 46.9%; Fisher's exact test, $p < 0.05$). Despite this, a different proportion of neurons was tuned to task features between the dorsal and ventral LPFC at 200 ms (χ = 11.37, $p < 0.01$), 600 ms ($\chi = 15.75$, $p < 0.01$), but not 1,000 ms ($\chi = 8.67$, $p = 0.07$). Ventral LPFC neurons were preferentially tuned to context and CPO earlier in the trial (explored in more detail below).

The latency with which individual neurons represented task features is summarized in Figure 3B. Neurons in the ventral LPFC acquired tuning to task features in the same temporal pattern: first context, then CPO, and finally the target side. In the ventral LPFC, neurons were tuned to the context with a mean latency (±SE) of 346.2 ± 47.4 ms in monkey B and 282.1 ± 66.1 ms in monkey T. Individual neurons then demonstrated CPO tuning significantly later relative to context (577.4 ± 42.4 ms, $p < 0.001$ in monkey B; 516.5 ± 75.8 ms, $p < 0.01$ in monkey T; Wilcoxon rank-sum test). Neurons finally acquired tuning to the target side (827.5 ± 18.1 ms, $p < 0.001$ in monkey B, 933.3 ± 31.8 ms, $p < 0.05$ in monkey T, Wilcoxon rank-sum test). Neurons in the dorsal LPFC had different tuning profiles in the two monkeys. The main difference for monkey B was that neurons in the dorsal LPFC were tuned to CPO closer in time (663.6 ± 33.4 ms) as tuning to the target side (738.6 ± 16.2 ms; p = 0.50). This suggests that, unlike in the ventral LPFC, neurons in monkey B's dorsal LPFC did not encode CPO prior to the target side or the allocation of attention/gaze to that side. Finally, monkey T had a limited number of neurons in the dorsal LPFC tuned to context and CPO, and therefore statistical testing comparing latency was not performed.

As mentioned previously, many neurons changed their tuning over the course of a trial. To further explore this, we considered all neurons that were first tuned to context prior to 400 ms and quantified the task features they represented at 600 and 1,000 ms (Figure 3C). The same analysis was performed for CPO, but tuning prior to 600 ms was considered. Neurons

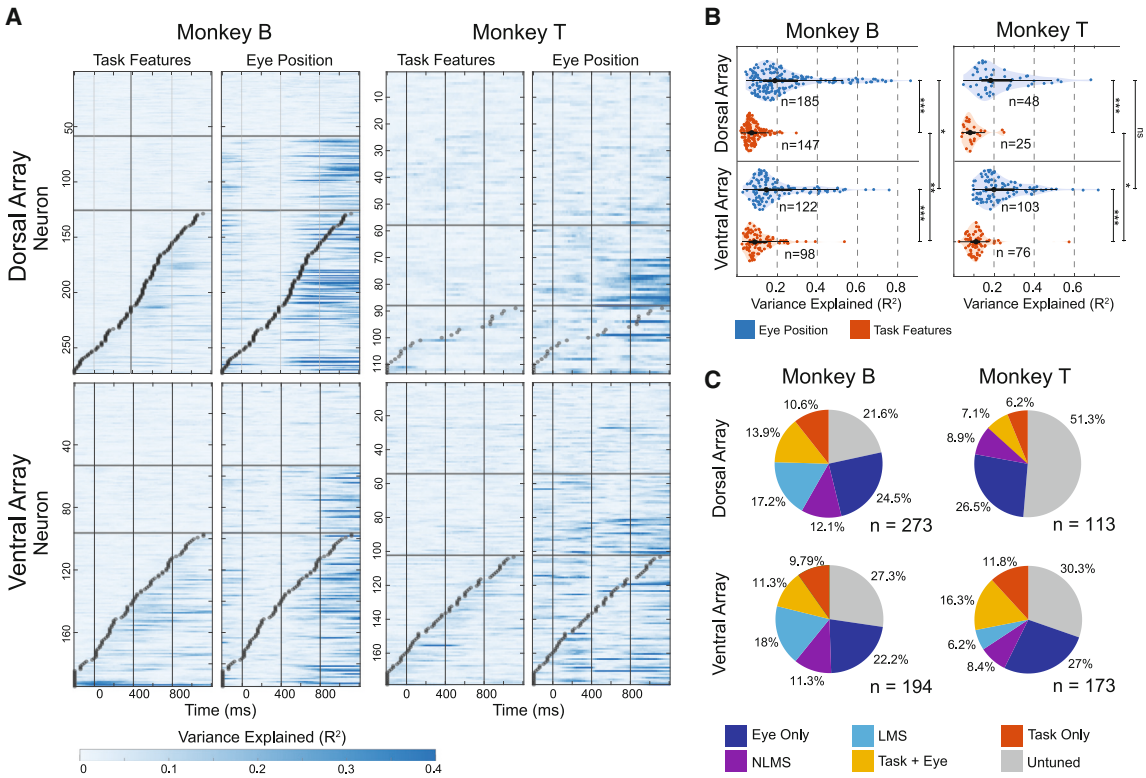

Figure 2. Activity of LPFC neurons is modulated by eye position and task features

(A) Manually isolated neurons were analyzed during goal onset over 400-ms windows overlapped by 20 ms, performed separately across the ventral and dorsal LPFC for each monkey. Heatmaps represent the variance of each neuron's activity, explained (R^2) by eye position and task features. Untuned neurons are at the top, with neurons only tuned to eye position below, and neurons tuned to task features at the bottom. For the neurons tuned to task features, the latency of their tuning is shown by a gray circle.

(B) Maximum R^2 during the trial epoch plotted for all neurons tuned to task features and eye position. R^2 for eye position and task features was compared within each array and compared separately across the two arrays (Wilcoxon rank-sum test; *n* for each group is indicated in the figure; non-significant (ns), $p > 0.05$; $^*p < 0.05$; $^{**}p < 0.01$; $^{***}p < 0.001$).

(C) To quantify the mixed tuning observed between eye position and task features in (A), neurons were categorized as linearly mixed selective (LMS), non-linearly mixed selective (NLMS), and tuned to task features and eye position at different times (task + eye). Otherwise, neurons were only tuned to task features (task only) or eye position (eye only) or were untuned.

demonstrated temporal mixed selectivity in monkey B, with only 5 of the 61 neurons (8.2%) maintaining context selectivity and 4 of the 39 neurons (10.2%) maintaining CPO selectivity at 1,000 ms across both arrays. Furthermore, most of the context neurons prior to 400 ms demonstrated selectivity to other features (35, 57.4%) at 1,000 ms in both arrays, and similarly, most of the CPO neurons prior to 600 ms were tuned to other task features (18, 51.4%). Only the ventral LPFC was assessed in monkey T, which also demonstrated dynamic tuning but limited mixed selectivity with other features over times (Figure 3C, bottom). Specifically, 21 of the 24 neurons (87.5%) initially tuned to context were untuned at 1,000 ms. This difference between the two animals may be related to monkey T's more limited use of eye position later in the trial (Figure S1A) and may be influenced by limited trial numbers (Figure S1C).

Decoding task features of ventral and dorsal LFPC neuronal ensembles across individual sessions

We found that individual neurons are dynamically tuned to task features. However, single-neuron analysis may not adequately capture the informational capacity of a population of simultaneously recorded units.[22] We therefore used a linear support vector machine (SVM) to classify task features from neuronal ensemble activity. We performed this analysis separately on each session, using sessions with at least 15 correct trials for each of the four conditions. We used firing rates integrated over the same 400-ms windows in steps of 20 ms around goal onset.

We trained and tested a linear SVM on normalized thresholded multiunit activity on each channel of the dorsal and ventral LPFC arrays (STAR Methods). The mean (±2SE) decoding performance across 12 sessions in monkey B and 8 sessions in monkey T is presented in Figure 4A. Each point is marked when the lower bound (mean – 2SE) exceeds chance performance. Task features could be decoded reliably following the same temporal pattern as observed with single-neuron tuning. This suggests that ensembles in the ventral LPFC represented context information throughout the task in both monkeys (orange traces in Figure 4A). Additionally, CPO could be decoded from the ventral LPFC after goal onset, followed by the target side. Only the target side could be decoded from the dorsal LPFC in monkey

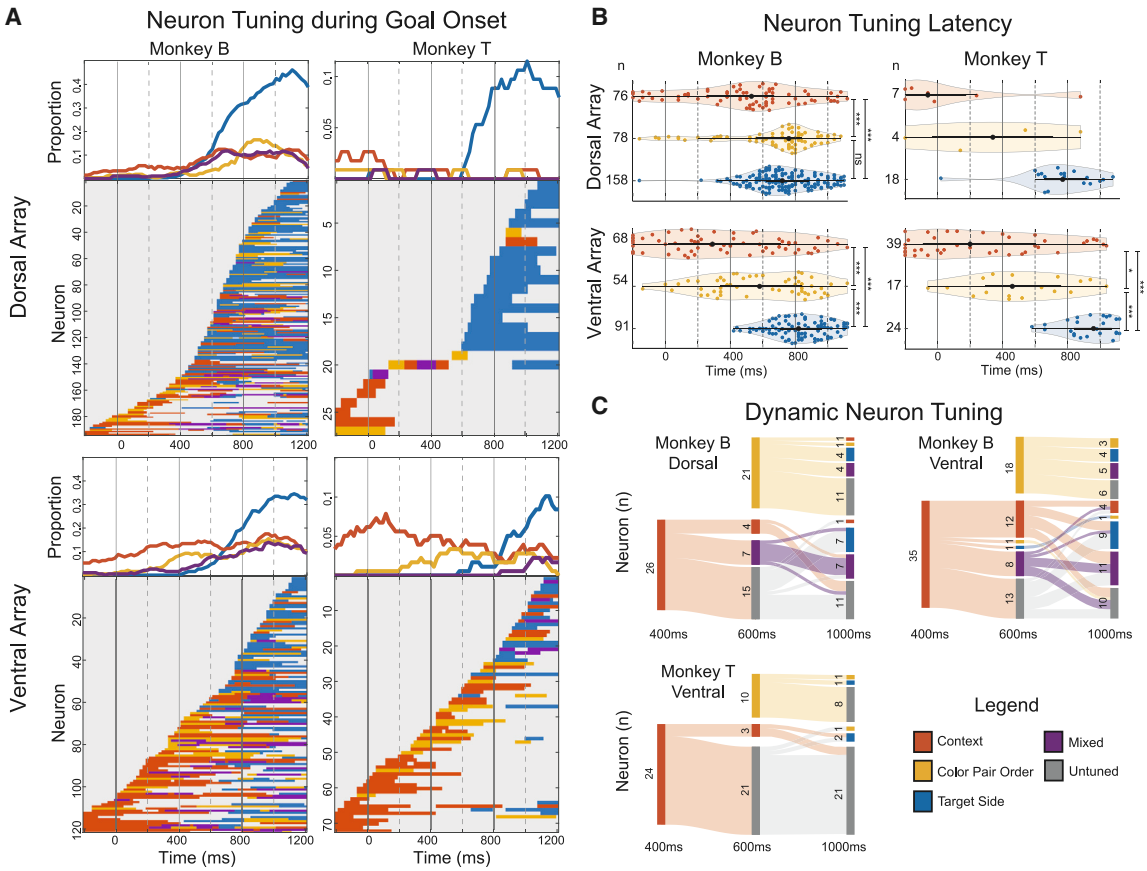

Figure 3. LPFC neurons temporally mix task features during virtual navigation

(A) Neuron tuning to specific task features is further characterized using the analysis performed in Figure 2. Top plots demonstrate the total number of neurons tuned to task features. Bottom plots represent each unit's tuning over time, sorted from bottom to top by onset of tuning to any feature.

(B) Latencies of all neurons tuned to task features in the ventral and dorsal PFC across both monkeys, with latencies compared using a Wilcoxon rank test; *n* for each group is indicated in the figure. ns, $p > 0.05$; *$p < 0.05$; ***$p < 0.001$.

(C) Dynamic neuron tuning was quantified for neurons that were first tuned to context prior to 400 ms and CPO prior to 600 ms. The proportion of these neurons tuned to different task features at 600 ms (for context) and 1,000 ms (for context and CPO) is illustrated using a Sankey diagram.

T (top right). However, context, CPO, and target side information could be decoded from the dorsal LPFC in monkey B (top left). These results were observed across individual sessions in monkeys B and T (Figure S3). Permutation testing with shuffled labels was used to obtain a 95% confidence interval for individual sessions (STAR Methods). We repeated the same ensemble analyses only including well-isolated single neurons. There was no significant difference (Wilcoxon rank-sum test) in decoding performance when training the classifier on multiunit activity and manually sorted spikes for both monkeys (Figure S4).

We then compared decoding accuracies of task features from the dorsal LPFC, ventral LPFC, and eye position using a Wilcoxon signed-rank test at three 400-ms intervals centered at 200, 600, and 1,000 ms after goal onset (Figures 4B and S5). Context information could be decoded more accurately from the ventral LPFC compared to eye position ($p < 0.001$ in monkey B, and $p < 0.01$ in monkey T, Wilcoxon signed-rank test) and the dorsal LPFC ($p < 0.001$ in monkey B and $p < 0.01$ in monkey T, Wilcoxon signed-rank test). CPO could also be decoded more accurately from the ventral LPFC compared to eye position at 600 ms ($p < 0.05$ in monkey B and $p < 0.05$ in monkey T, Wilcoxon signed-rank test) and the dorsal LPFC ($p = 0.05$ in monkey B and $p < 0.01$ in monkey T, Wilcoxon signed-rank test). Given monkey B's bias to fixate on one color in some sessions (Figure S2), we performed a Spearman's rank correlation between decoding accuracy from eye position compared to neural activity (Figure 4C). CPO information was independent of eye position only in the ventral LPFC at 600 ms, consistent with our single-neuron findings (Figure S1B).

Task features are represented dynamically in the ventral LPFC

Our population-level analysis shows that neural ensembles represent task features following the flow of information during task trials or the cognitive operations the animal needs to perform the task. Individual neurons also dynamically represented task features, with different neurons acquiring or modulating their tuning throughout a trial (Figure 3). These temporal multiplexing of features would predict that the neural codes across the different trial periods are dynamic and likely do not

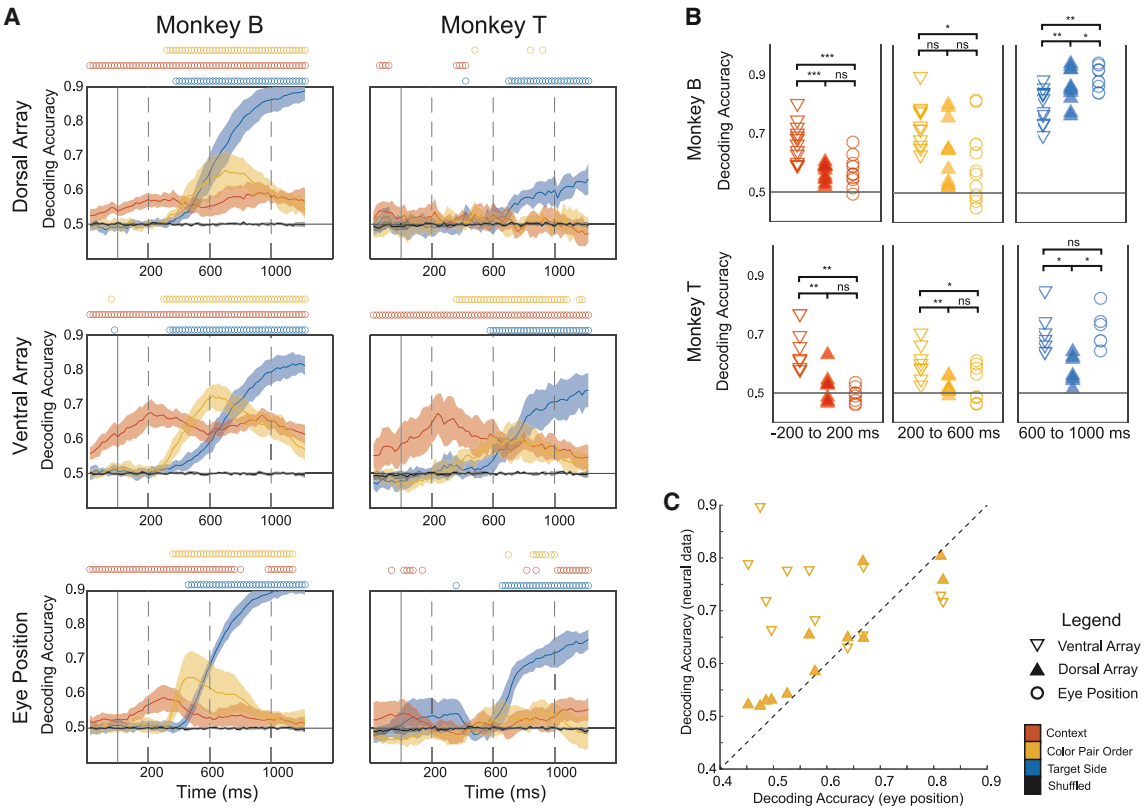

Figure 4. Decoding task features of ventral and dorsal LFPC neuronal ensembles across individual sessions

(A) Mean decoding accuracies of task features across 12 sessions (monkey B) and 8 sessions (monkey T) over 400-ms windows overlapped by 20 ms. This was performed separately for neural activity in the dorsal and ventral LPFC (mean and normalized multiunit activity) and mean eye position (mean x and y positions) over the same time epochs. Plots show mean (±2SE) decoding accuracy across sessions, with a circle above when the lower bound (mean − 2SE) exceeds chance performance.

(B) Comparing decoding accuracy across the ventral LPFC, dorsal LPFC, and eye position using a Wilcoxon signed-rank test (n = 12 for monkey B, n = 8 for monkey T). ns, $p > 0.05$; *$p < 0.05$; **$p < 0.01$; ***$p < 0.001$.

(C) Correlating decoding accuracy of CPO from eye position and neural data 600 ms (200–600 ms) after goal onset using Spearman's rank correlation. Decoding accuracy of CPO from eye position was highly correlated with accuracy from the dorsal LPFC (r(12) = 0.918, $p < 0.001$) but not from the ventral LPFC (r(12) = −0.329, $p = 0.30$).

generalize from one period to another. To investigate this issue, we trained a linear SVM to classify task features at each 400-ms window and tested this at the other different time windows (Figures 5, S6, and S7).

Context information was represented with a dynamic neural code (Figures 5A, top, and 5B). Context could be decoded more accurately at 200 ms from goal onset when the classifier was trained at that time compared to later in the epoch at 600 ms and 1,000 ms in both monkeys ($p < 0.001$ in monkey B, $p < 0.05$ in monkey T, Wilcoxon signed-rank test) (Figure 5C). Conversely, context was decoded more accurately at 1 000 ms from a classifier trained at that time compared to one trained at 200 ms ($p < 0.001$ in monkey B, $p < 0.05$ in monkey T, Wilcoxon signed-rank test) (Figure 5C). Target side information was represented by a more persistent code (Figure 5A, center), with no difference in decoding accuracy at 600 ms when trained at that time or at 1,000 ms in both monkeys (Figures S6 and S7). Finally, CPO demonstrated a partially dynamic neural code (Figure 5C, center column). Training a linear decoder to classify this feature at 600 ms demonstrated increased decoding accuracy at that time compared to a classifier trained at 1,000 ms ($p < 0.01$ in monkey B, $p < 0.05$ in monkey T, Wilcoxon signed-rank test); however, testing at 1,000 ms demonstrated the same accuracy as when trained at 600 ms and 1,000 ms ($p > 0.05$ in both monkeys, Wilcoxon signed-rank test). This suggests that there was a greater representation of CPO at 600 ms, but there was no additional CPO information present at 1,000 ms. To rule out a bias in eye position influencing this feature in monkey B, we only used sessions (n = 8) where he had no significant bias to fixate on one color. Although this limits the bias of eye position, it likely does not completely remove it and may explain some of the cross-temporal decoding differences observed in both the dorsal and ventral LPFC (Figure S6).

The LPFC represents task conditions and eye position in different subspaces

Our previous results indicate that individual neurons are modulated by both eye position and task features, mixing these

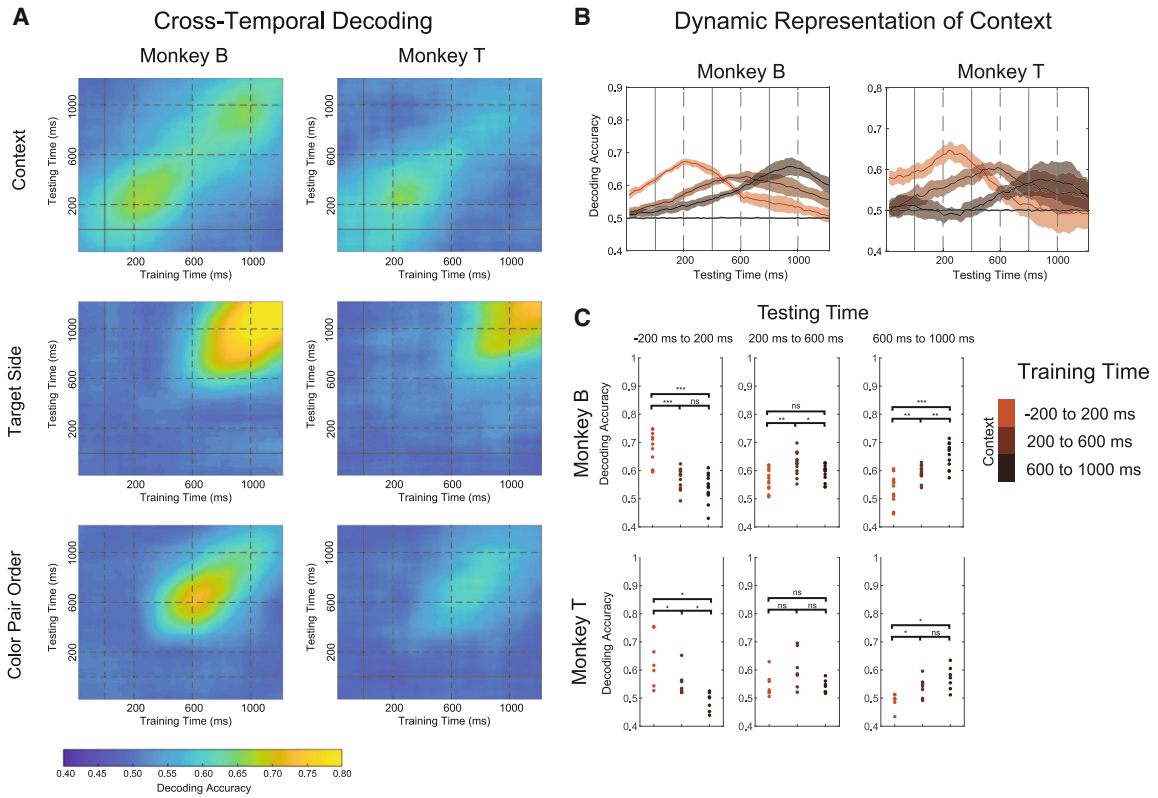

Figure 5. Task features are dynamically represented by neural ensembles in the ventral LPFC

(A) Cross-temporal decoding in the ventral LPFC, training a linear SVM on task features across 400-ms windows overlapped by 20 ms and testing each model on 400-ms windows overlapped by 20 ms across the whole epoch. Heatmaps show mean decoding accuracies across 12 sessions in monkey B and 8 sessions in monkey T.

(B) Mean (±2SE) decoding accuracy of the task's context across time when trained at 200, 600, and 1,000 ms.

(C) Comparing decoding accuracies of models trained at 200, 600, and 1,000 ms when testing on different time windows. Decoding accuracies were compared using a Wilcoxon signed-rank test (n = 12 for monkey B, n = 8 for monkey T). ns, $p > 0.05$; *$p < 0.05$; **$p < 0.01$; ***$p < 0.001$.

elements over time (Figures 2 and 3). Despite this, neural populations must be able to represent and separate relevant features under naturalistic conditions. We explored this further by examining the dimensionality of neural activity in six novel sessions from monkey B. Neural data projected on the top 30 principal components (PCs; STAR Methods) were used in subsequent analyses. The same analysis was performed using neural activity at individual times and by concatenating times and trials (Figure S8). We first identified an axis that explained eye position on the x axis (Eye_x) using a multivariable linear regression. Projecting averaged neural activity from left-out trials on this axis demonstrates a significant correlation with Eye_x (Figure 6A). Furthermore, the Euclidean distance on this axis was significantly greater in the dorsal LPFC compared to the ventral LPFC ($p < 0.05$ at 600 ms, $p < 0.01$ at 1,000 ms, Wilcoxon rank-sum test) across all conditions (n = 24).

To find axes that separated task conditions, we used linear discriminant analysis on the null space of the Eye_x dimension (i.e., the 29 orthogonal axes). This was done to limit the bias of eye position and can demonstrate that task features are represented in a different subspace. The mean neural activity across separate conditions projected on the context and CPO axes can be visualized over time in Figure 6B. This activity separated along the context and CPO axes, as characterized previously, but this analysis allowed us to quantify the variance of population activity explained by task features (Figure S8). We noticed that the right conditions separated more along context and CPO axes compared to left conditions at 1,000 ms (Euclidean distance compared, $p < 0.01$, Wilcoxon rank-sum test). Exploring this further, it was noted that some sessions had a significant bias to choose the left side, resulting in more of those trials being correct by chance. This is demonstrated in two sessions with strong (session 5) and weak (session 2) biases by plotting the proportion of correct responses separately per condition (Figure 6C). Plotting Euclidean distance of neural activity projected on the context and CPO axes demonstrated significantly less separation in the left compared to right conditions ($p < 0.001$ at 600, 800, and 1,000 ms; Wilcoxon rank-sum test) across trials (Figure 6C). Finally, this was not the case at 600 and 800 ms in session 2, but there was a significant difference at 1,000 ms ($p < 0.05$, Wilcoxon rank-sum test). This is likely driven by the steel condition, where a slight left bias was present.

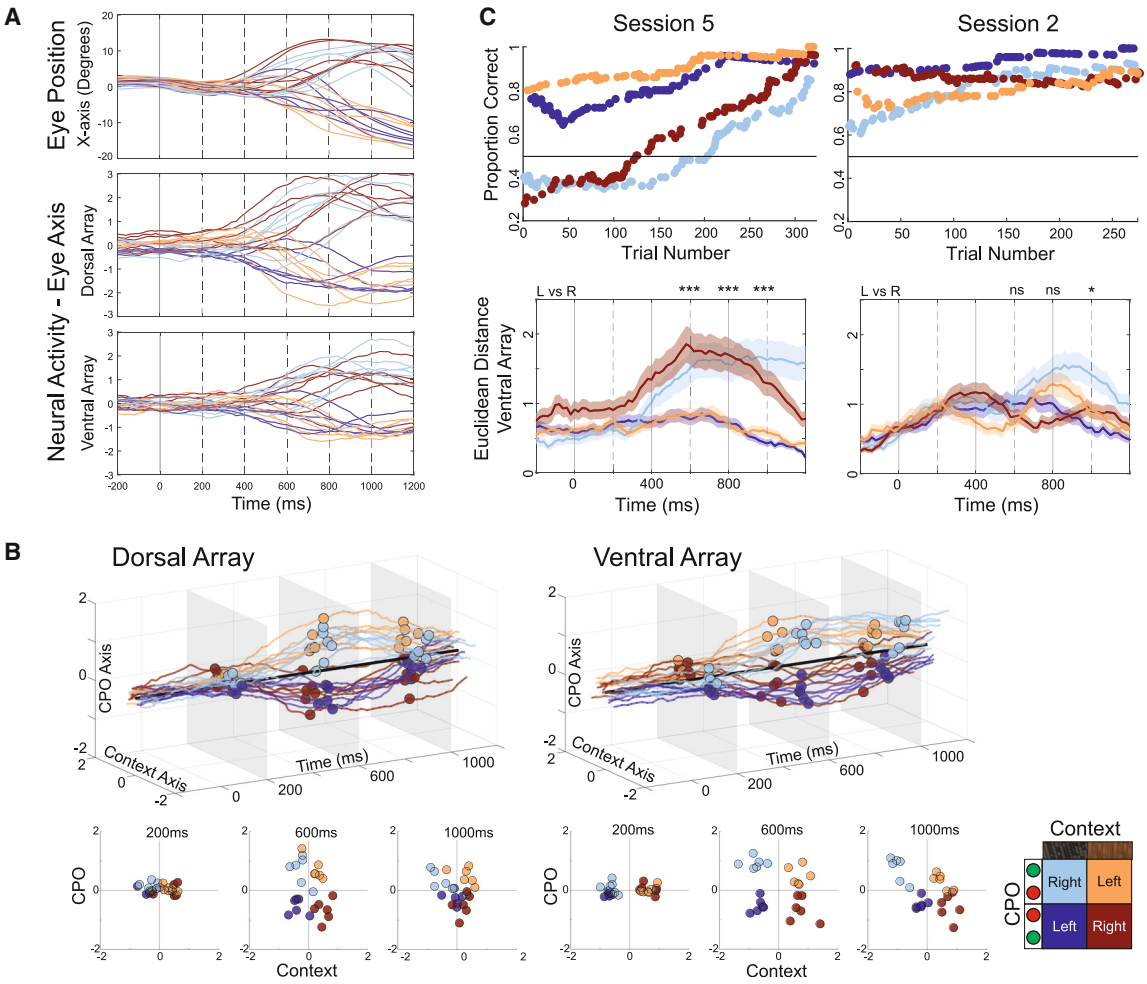

Figure 6. Neural activity separates task conditions along task-related dimensions

(A) Eye position along the x axis across six sessions (top) along with neural activity projected on the eye position axis for the dorsal and ventral LPFC.

(B) Separation along task feature axes over time, where task feature axes were computed in the null space of the eye position axis. Projection on these axes is shown at 200, 600, and 1,000 ms. Greater separation along task features can be observed in the ventral LPFC, and this separation was maximized at 600 ms. Furthermore, the ventral LPFC separated the right conditions significantly more than the left conditions at 1,000 ms ($p < 0.01$, Wilcoxon rank-sum test, $n = 12$ conditions in each group).

(C) Two example sessions with a large bias to choose the left side (session 5, left) and a minimal bias in choosing the left side under the steel conditions (session 2, right). Mean Euclidean distance (±SE) across all correct trials in each session is plotted over time. Right conditions separately significantly more than left conditions in session 5 (Wilcoxon rank-sum test, $n = 89$ right trials, $n = 141$ left trials) at 600, 800, and 1,000 ms and only in the steel conditions in session 2 (Wilcoxon rank-sum test, $n = 121$ right trials, $n = 114$ left trials). Ns, $p > 0.05$; *$p < 0.05$; ***$p < 0.001$.

DISCUSSION

We recorded single-neuron responses in the dorsal and ventral LPFC of macaques while the animals navigated a virtual environment and performed an associative memory task with variable spatiotemporal structure. Our main results were that (1) single neurons in the LPFC show mixed selectivity for task relevant features and eye position, (2) single neurons and ensembles were dynamically selective for the different elements of the task depending on the time relevance of that element to solve the task, and (3) while neurons in the ventral LPFC encoded spatial and non-spatial features, neurons in the dorsal LPFC mainly encoded spatial information.

Neural dynamics in a naturalistic setting

Few studies have examined single-neuron tuning in the primate LPFC in naturalistic settings. During most experiments, eye position is strictly controlled, and stimuli are presented on a stationary background. In these studies, animals do not have the ability to change their view or position in the environment and therefore cannot control the spatiotemporal dynamic of task elements. These restrictions have served as important controls limiting experimental confounds but also limit the ability to generalize findings to many real-world scenarios. We reasoned that the LPFC must perform its function in complex environments in the presence of gaze movements and changing scenery. One study[19] trained monkeys to perform a simple associative

memory task without limiting the animals' head and eye movements. They showed that coding of relevant features in the LPFC was robust and not degraded by unstructured movements. Although this work is an important step toward understanding neural representations in naturalistic settings, it did not explore neuron tuning in a complex environment such as the one in our task, where features changed as the animal voluntarily moved through the environment. This capacity to execute actions that cause a change in the virtual world is referred to as a feeling of agency.[23] Other studies have used virtual environments as a surrogate for real-world naturalistic settings and reported tuning for spatial working memory in the LPFC and for stimulus features in the hippocampus.[20,21,24–26] This factor should not be underestimated, since here, animals do not act as passive observers but as actors, triggering task events at variable times during the trial.

Unconstrained naturalistic tasks in which subjects have agency may provide insights into the neural dynamics of the LPFC during real-world conditions. We showed that single neurons in the ventral LFPC were serially tuned to relevant task features as they "appear" in a naturalistic associative memory task: first representing context, followed by the CPO, and finally target location. Interestingly, neurons largely acquired tuning to the context shortly before the goal was triggered (Figure 3), despite this information being previously available, suggesting that context was only represented in the LPFC when becoming immediately relevant. Furthermore, these neural representations were dynamic over time, both at the single-neuron (Figure 3) and ensemble level (Figures 5 and 6). Single neurons in the LPFC have been observed to non-linearly mix task-relevant features, allowing for flexible high-dimensional representations that can be read out from downstream cortical areas.[6,7,27,28] Our results support these findings and show that task features are represented in separate subspace than unconstrained features such as eye position. This could explain how neural populations can represent and manipulate information without being affected by variable elements in a naturalistic setting. Furthermore, we show that neuron tuning is dynamic over time (Figure 3B). Such dynamics coding has been observed in the rodent hippocampus during virtual navigation,[29] allowing for the tuning of episodic sequences by the same population of neurons. In the LPFC, possible advantages of dynamic coding include utilizing the same neurons to represent individual features, the combination of those features united by rules,[5,30–32] and a dynamic representation of a spatiotemporal episode.[33]

Anatomical and functional subdivision of LPFC

The neural dynamics discussed previously were mostly found in the ventral LPFC in both monkeys tested, suggesting a functional division within this region. The ventral and dorsal LPFC had different tuning profiles while the monkeys completed the task, with more neurons in the ventral LPFC being tuned to visual and visuospatial features. The ordered tuning of context, target location, and target side was observed only in the ventral LPFC (Figure 3B). These results suggest that the ventral LPFC is more likely to represent visual features when compared to the dorsal LPFC. These results are consistent with connectivity studies showing that there is dorsal and ventral mapping of the LPFC to corresponding dorsal and ventral high-level visual areas.[1,9–11] Here, we should clarify that our mapping of the ventral LPFC was not anatomically precise, and it may include area 46 and some portions of area 45, which include main projections from the ventral visual processing stream.[1,9,10]

Other single-neuron studies have demonstrated more mixed results regarding a functional organization of the LPFC.[5,6,12–17] In contrast, we observe a relatively robust difference between single-neuron tuning and ensemble dynamics between the ventral and dorsal LFPC. The increased cognitive demands of interpreting a complex scene and freely navigating through it may exacerbate underlying regional specializations in function. This study examines anatomical differences in LPFC function at the single-neuron and population levels during a virtual associative memory and navigation task. Importantly, our study demonstrates that it is possible to use a virtual task to explore information processing in monkey LPFC neurons and offers insights into the dynamic nature of their mixed selectivity.

Our results have implications for models of LPFC function and interactions with the rest of the brain. Interestingly, one recent study has shown that stimulation of the LPFC evokes selective activation of specific regions in associative areas of the neocortex.[11] The connectivity of the LPFC with early sensory areas was practically non-existent, suggesting that the LPFC mainly receives integrated information from association areas. Because the mixing of features is not solely a feature of the LPFC but may start in association cortices, the information that LPFC neurons integrate could be highly filtered, and features may be already mixed. The latter may facilitate the multiplexing time dynamics of relevant features observed in our study as well as how feedback signals from the LPFC may reach association areas. Thus, the reported role of the LPFC on several components of cognitive control, such as attention,[34–37] working memory,[20] perception,[38] rule coding,[21,31,39] and planning[40] (see Miller[41] for a review), could be understood in neurophysiological terms as containing populations of neurons that can serve as spatiotemporal integrators of information held in the focus of perceptual awareness. Interestingly a recent study has reported that neurons in the LPFC encode paths toward a remembered location via neural activation sequences.[42] Thus, the LPFC may integrate information that has variable spatiotemporal structure. This may enable the high level of mental abstraction during planning observed in anthropoid primates[43] with large prefrontal cortices.

Limitations of the study

Having a naturalistic task necessitated unrestricted eye movements, which provided some confounds to our task. We mitigated this by removing eye position information in our single-neuron analysis and comparing the decoding accuracy of neural activity to that of eye position. Despite this, we were unable to dissociate eye position, mostly driven by the side fixated on, from the decision variable. It is unclear when the decision would have occurred in this naturalistic setting and possibly occurred between fixation and reaction time indicated by moving the joystick (Figure S1). However, even with a conservative estimate that this occurs during fixation, we show that CPO is represented prior to this in the ventral LPFC and not dorsal LPFC. This

suggests that the ventral LPFC may be involved in the computation required prior to the decision. Additionally, the interaction of our task elements (context and CPO) in correct trials was the same as the target side (Figure 1), limiting our ability to investigate non-linear mixed selectivity between context and CPO. This could be mitigated by using incorrect trials, which were limited in our case, or by changing the rule. However, the complexity of navigating freely while performing a cognitive task potentially resulted in variable learning behaviors without introducing a rule change (Figure S1). Finally, eye movements and overt attention are highly correlated. In tasks such as ours, it is difficult to dissociate eye position and attention, which is usually done in covert attention tasks. Our task may better approximate natural behavior, but this dissociation becomes more problematic than in other reductionist tasks. However, in spite of the aforementioned limitations, our results provide insights into how LPFC neural activity encodes task variables during naturalistic tasks.

RESOURCE AVAILABILITY

Lead contact

Requests for further information and resources should be directed to and will be fulfilled by the lead contact, Julio Martinez-Trujillo (julio.martinez@robarts.ca).

Materials availability

All data reported in this paper will be shared by the lead contact upon request.

Data and code availability

- All data reported in this paper will be shared by the lead contact upon request.
- All original code will be available at https://doi.org/10.5281/zenodo.10520991.
- Any additional information required to reanalyze the data reported in this paper is available from the lead contact upon request.

ACKNOWLEDGMENTS

We thank B. Bally, K. Barker, J. Blonde, S. Chisling, R. Kersten, W. Kucharski, S. Nuara, and K. Thomas for technical assistance. This work was supported by the Natural Sciences and Engineering Research Council of Canada Postdoctoral Scholarship, the Ontario Graduate Scholarship, and the Clinician Investigator Program Stipend at Western University. Additionally, this work was funded by the Canadian Institutes of Health Research, NSERC, BrainsCAN, and NEURONEX Brain Initiative (ref. FL6GV84CKN57) grants (to J.C.M.).

AUTHOR CONTRIBUTIONS

M.A. analyzed data, interpreted data, and wrote the manuscript. B.C. designed the task, collected data, and contributed to data interpretation and manuscript writing. R.J. contributed to data analysis and data interpretation. R.G. designed the task and collected data. A.S. contributed to surgical implantation and data interpretation. J.C.L. contributed to data interpretation. J.M.-T. contributed to task design, surgical implantation, data analysis, data interpretation, and manuscript writing.

DECLARATION OF INTERESTS

The authors declare no competing interests.

STAR★METHODS

Detailed methods are provided in the online version of this paper and include the following:

- KEY RESOURCES TABLE
- EXPERIMENTAL MODEL AND STUDY PARTICIPANT DETAILS
- METHOD DETAILS
  - Electrophysiological recordings
  - Experimental setup
  - Behavioral tasks
- QUANTIFICATION AND STATISTICAL ANALYSIS
  - Behavioral analysis
  - Single neuron tuning
  - Decoding from population neural activity
  - Cross-temporal decoding analysis
  - Dimensionality reduction and state-space analysis

SUPPLEMENTAL INFORMATION

Supplemental information can be found online at https://doi.org/10.1016/j.celrep.2024.115124.

Received: February 15, 2024
Revised: June 11, 2024
Accepted: December 9, 2024
Published: January 7, 2025

REFERENCES

1. Petrides, M. (2005). Lateral prefrontal cortex: architectonic and functional organization. Philos. Trans. R. Soc. Lond. B Biol. Sci. *360*, 781–795. https://doi.org/10.1098/rstb.2005.1631.
2. Miller, E.K., and Cohen, J.D. (2001). An Integrative Theory of Prefrontal Cortex Function. Annu. Rev. Neurosci. *24*, 167–202. https://doi.org/10.1146/annurev.neuro.24.1.167.
3. Duncan, J. (2001). An adaptive coding model of neural function in prefrontal cortex. Nat. Rev. Neurosci. *2*, 820–829. https://doi.org/10.1038/35097575.
4. Mansouri, F.A., Freedman, D.J., and Buckley, M.J. (2020). Emergence of abstract rules in the primate brain. Nat. Rev. Neurosci. *21*, 595–610. https://doi.org/10.1038/s41583-020-0364-5.
5. Wallis, J.D., Anderson, K.C., and Miller, E.K. (2001). Single neurons in prefrontal cortex encode abstract rules. Nature *411*, 953–956. https://doi.org/10.1038/35082081.
6. Asaad, W.F., Rainer, G., and Miller, E.K. (1998). Neural activity in the primate prefrontal cortex during associative learning. Neuron *21*, 1399–1407. https://doi.org/10.1016/s0896-6273(00)80658-3.
7. Rigotti, M., Barak, O., Warden, M.R., Wang, X.-J., Daw, N.D., Miller, E.K., and Fusi, S. (2013). The importance of mixed selectivity in complex cognitive tasks. Nature *497*, 585–590. https://doi.org/10.1038/nature12160.
8. Parthasarathy, A., Herikstad, R., Bong, J.H., Medina, F.S., Libedinsky, C., and Yen, S.-C. (2017). Mixed selectivity morphs population codes in prefrontal cortex. Nat. Neurosci. *20*, 1770–1779. https://doi.org/10.1038/s41593-017-0003-2.
9. Barbas, H., and Pandya, D.N. (1989). Architecture and intrinsic connections of the prefrontal cortex in the rhesus monkey. J. Comp. Neurol. *286*, 353–375. https://doi.org/10.1002/cne.902860306.
10. Barbas, H. (2015). General Cortical and Special Prefrontal Connections: Principles from Structure to Function. Annu. Rev. Neurosci. *38*, 269–289. https://doi.org/10.1146/annurev-neuro-071714-033936.
11. Xu, R., Bichot, N.P., Takahashi, A., and Desimone, R. (2022). The cortical connectome of primate lateral prefrontal cortex. Neuron *110*, 312–327. https://doi.org/10.1016/J.NEURON.2021.10.018.
12. Riley, M.R., Qi, X.-L., and Constantinidis, C. (2017). Functional specialization of areas along the anterior–posterior axis of the primate prefrontal cortex. Cerebr. Cortex *27*, 3683–3697. https://doi.org/10.1093/cercor/bhw190.

13. Meyer, T., Qi, X.-L., Stanford, T.R., and Constantinidis, C. (2011). Stimulus Selectivity in Dorsal and Ventral Prefrontal Cortex after Training in Working Memory Tasks. J. Neurosci. *31*, 6266–6276. https://doi.org/10.1523/JNEUROSCI.6798-10.2011.

14. O'Reilly, R.C. (2010). The What and how of prefrontal cortical organization. Trends Neurosci. *33*, 355–361. https://doi.org/10.1016/j.tins.2010.05.002.

15. Kadohisa, M., Kusunoki, M., Petrov, P., Sigala, N., Buckley, M.J., Gaffan, D., and Duncan, J. (2015). Spatial and temporal distribution of visual information coding in lateral prefrontal cortex. Eur. J. Neurosci. *41*, 89–96. https://doi.org/10.1111/ejn.12754.

16. Siegel, M., Buschman, T.J., and Miller, E.K. (2015). Cortical information flow during flexible sensorimotor decisions. Science *348*, 1352–1355. https://doi.org/10.1126/science.aab0551.

17. Tang, H., Bartolo, R., and Averbeck, B.B. (2021). Reward-related choices determine information timing and flow across macaque lateral prefrontal cortex. Nat. Commun. *12*, 894. https://doi.org/10.1038/s41467-021-20943-9.

18. Rouzitalab, A., Boulay, C.B., Park, J., Martinez-Trujillo, J.C., and Sachs, A.J. (2023). Ensembles code for associative learning in the primate lateral prefrontal cortex. Cell Rep. *42*, 112449. https://doi.org/10.1016/j.celrep.2023.112449.

19. Tremblay, S., Testard, C., DiTullio, R.W., Inchauspé, J., and Petrides, M. (2023). Neural cognitive signals during spontaneous movements in the macaque. Nat. Neurosci. *26*, 295–305. https://doi.org/10.1038/s41593-022-01220-4.

20. Roussy, M., Luna, R., Duong, L., Corrigan, B., Gulli, R.A., Nogueira, R., Moreno-Bote, R., Sachs, A.J., Palaniyappan, L., and Martinez-Trujillo, J.C. (2021). Ketamine disrupts naturalistic coding of working memory in primate lateral prefrontal cortex networks. Mol. Psychiatr. *26*, 6688–6703. https://doi.org/10.1038/s41380-021-01082-5.

21. Corrigan, B.W., Gulli, R.A., Doucet, G., Roussy, M., Luna, R., Pradeepan, K.S., Sachs, A.J., and Martinez-Trujillo, J.C. (2022). Distinct neural codes in primate hippocampus and lateral prefrontal cortex during associative learning in virtual environments. Neuron *110*, 2155–2169. https://doi.org/10.1016/j.neuron.2022.04.016.

22. Tremblay, S., Pieper, F., Sachs, A., and Martinez-Trujillo, J. (2015). Attentional Filtering of Visual Information by Neuronal Ensembles in the Primate Lateral Prefrontal Cortex. Neuron *85*, 202–215. https://doi.org/10.1016/j.neuron.2014.11.021.

23. Bódi, B. (2022). Videogames and Agency (Routledge). https://doi.org/10.4324/9781003298786.

24. Johnston, R., Abbass, M., Corrigan, B., Gulli, R., Martinez-Trujillo, J., and Sachs, A. (2023). Decoding spatial locations from primate lateral prefrontal cortex neural activity during virtual navigation. J. Neural. Eng. *20*, 016054. https://doi.org/10.1088/1741-2552/acb5c2.

25. Gulli, R.A., Duong, L.R., Corrigan, B.W., Doucet, G., Williams, S., Fusi, S., and Martinez-Trujillo, J.C. (2020). Context-dependent representations of objects and space in the primate hippocampus during virtual navigation. Nat. Neurosci. *23*, 103–112. https://doi.org/10.1038/s41593-019-0548-3.

26. Wirth, S., Baraduc, P., Planté, A., Pinède, S., and Duhamel, J.-R. (2017). Gaze-informed, task-situated representation of space in primate hippocampus during virtual navigation. PLoS Biol. *15*, e2001045. https://doi.org/10.1371/journal.pbio.2001045.

27. Fusi, S., Miller, E.K., and Rigotti, M. (2016). Why neurons mix: high dimensionality for higher cognition. Curr. Opin. Neurobiol. *37*, 66–74. https://doi.org/10.1016/j.conb.2016.01.010.

28. Dang, W., Jaffe, R.J., Qi, X.-L., and Constantinidis, C. (2021). Emergence of Non-Linear Mixed Selectivity in Prefrontal Cortex after Training. J. Neurosci. *41*, 7420–7434. https://doi.org/10.1523/JNEUROSCI.2814-20.2021.

29. Moore, J.J., Cushman, J.D., Acharya, L., Popeney, B., and Mehta, M.R. (2021). Linking hippocampal multiplexed tuning, Hebbian plasticity and navigation. Nature *599*, 442–448. https://doi.org/10.1038/s41586-021-03989-z.

30. Tanji, J., and Hoshi, E. (2008). Role of the Lateral Prefrontal Cortex in Executive Behavioral Control. Physiol. Rev. *88*, 37–57. https://doi.org/10.1152/physrev.00014.2007.

31. Buckley, M.J., Mansouri, F.A., Hoda, H., Mahboubi, M., Browning, P.G.F., Kwok, S.C., Phillips, A., and Tanaka, K. (2009). Dissociable Components of Rule-Guided Behavior Depend on Distinct Medial and Prefrontal Regions. Science *325*, 52–58. https://doi.org/10.1126/science.1172377.

32. Mendoza-Halliday, D., and Martinez-Trujillo, J.C. (2017). Neuronal population coding of perceived and memorized visual features in the lateral prefrontal cortex. Nat. Commun. *8*, 15471. https://doi.org/10.1038/ncomms15471.

33. Roussy, M., Busch, A., Luna, R., Leavitt, M.L., Mofrad, M.H., Gulli, R.A., Corrigan, B., Mináč, J., Sachs, A.J., Palaniyappan, L., et al. (2022). Neural sequences in primate prefrontal cortex encode working memory in naturalistic environments. Preprint at bioRxiv. https://doi.org/10.1101/2022.08.18.504406.

34. Bichot, N.P., Heard, M.T., DeGennaro, E.M., and Desimone, R. (2015). A Source for Feature-Based Attention in the Prefrontal Cortex. Neuron *88*, 832–844. https://doi.org/10.1016/j.neuron.2015.10.001.

35. Backen, T., Treue, S., and Martinez-Trujillo, J.C. (2018). Encoding of Spatial Attention by Primate Prefrontal Cortex Neuronal Ensembles. eNeuro *5*, 372–416. https://doi.org/10.1523/ENEURO.0372-16.2017.

36. Duong, L., Leavitt, M., Pieper, F., Sachs, A., and Martinez-Trujillo, J. (2019). A Normalization Circuit Underlying Coding of Spatial Attention in Primate Lateral Prefrontal Cortex. eNeuro *6*, 301–318. https://doi.org/10.1523/ENEURO.0301-18.2019.

37. Lennert, T., and Martinez-Trujillo, J. (2011). Strength of Response Suppression to Distracter Stimuli Determines Attentional-Filtering Performance in Primate Prefrontal Neurons. Neuron *70*, 141–152. https://doi.org/10.1016/j.neuron.2011.02.041.

38. Mendoza-Halliday, D., Torres, S., Desimone, R., and Martinez-Trujillo, J. (2018). Functional and anatomical characterization of visual working memory coding. J. Vis. *18*, 106. https://doi.org/10.1167/18.10.106.

39. Kaping, D., Vinck, M., Hutchison, R.M., Everling, S., and Womelsdorf, T. (2011). Specific Contributions of Ventromedial, Anterior Cingulate, and Lateral Prefrontal Cortex for Attentional Selection and Stimulus Valuation. PLoS Biol. *9*, e1001224. https://doi.org/10.1371/journal.pbio.1001224.

40. Tanji, J., Shima, K., and Mushiake, H. (2007). Concept-based behavioral planning and the lateral prefrontal cortex. Trends Cognit. Sci. *11*, 528–534. https://doi.org/10.1016/j.tics.2007.09.007.

41. Miller, E.K. (2000). The prefontral cortex and cognitive control. Nat. Rev. Neurosci. *1*, 59–65. https://doi.org/10.1038/35036228.

42. Busch, A., Roussy, M., Luna, R., Leavitt, M.L., Mofrad, M.H., Gulli, R.A., Corrigan, B., Mináč, J., Sachs, A.J., Palaniyappan, L., et al. (2024). Neuronal activation sequences in lateral prefrontal cortex encode visuospatial working memory during virtual navigation. Nat. Commun. *15*, 4471. https://doi.org/10.1038/s41467-024-48664-9.

43. Passingham, R.E., and Wise, S.P. (2012). The Neurobiology of the Prefrontal Cortex (Oxford University Press). https://doi.org/10.1093/acprof:osobl/9780199552917.001.0001.

44. Doucet, G., Gulli, R.A., and Martinez-Trujillo, J.C. (2016). Cross-species 3D virtual reality toolbox for visual and cognitive experiments. J. Neurosci. Methods *266*, 84–93. https://doi.org/10.1016/j.jneumeth.2016.03.009.

45. Ravassard, P., Kees, A., Willers, B., Ho, D., Aharoni, D.A., Cushman, J., Aghajan, Z.M., and Mehta, M.R. (2013). Multisensory Control of Hippocampal Spatiotemporal Selectivity. Science *340*, 1342–1346. https://doi.org/10.1126/science.1232655.

STAR★METHODS

KEY RESOURCES TABLE

REAGENT or RESOURCE	SOURCE	IDENTIFIER
Deposited data		
Raw and analyzed data	This paper	https://doi.org/10.5281/zenodo.10520991
Experimental models: Organisms/strains		
Rhesus Macaques	Unspecified	Western University
Software and algorithms		
MATLAB 2020a	MathWorks	http://www.mathworks.com/products/matlab/ RRID:SCR_001622
Offline Sorter	Plexon	https://plexon.com/products/offlinesorter/ RRID:SCR_000012
Other		
Utah Microelectrode Arrays	Blackrock Microsystems	https://blackrockneurotech.com/research/utah-array/
Original code	This paper	https://doi.org/10.5281/zenodo.10520991

EXPERIMENTAL MODEL AND STUDY PARTICIPANT DETAILS

Two male rhesus macaques (*Macaca mulatta*; 7 and 14 years old, 7kg and 12kg respectively) were used in these experiments. The monkeys were trained to perform a virtual reality associative memory task and received a juice reward as a form of positive reinforcement for each session. All animal procedures were compliant with the Canadian Council on Animal Care guidelines and approved by the Western University Animal Care Committee.

METHOD DETAILS

Electrophysiological recordings

Lateral prefrontal cortical (LPFC) recordings were acquired using two 96-channel Utah arrays for each animal (Blackrock Microsystems). Each animal received a 3-Tesla T1-weighted MRI which was used for surgical navigation using Brainsight (Rogue Research Inc.). The Utah arrays were positioned just anterior to the arcuate sulcus, with one placed dorsal to the principal sulcus (areas 46d/9d) and one placed ventral to the principal sulcus (areas 46v/9v). Each shank was 1.5mm and was therefore likely in layers II/III. Intraoperative images of the arrays' positions for each animal are presented in Figure 1A, with the corresponding regions highlighted in the MRI scans. Signals were obtained at 30kHz using a Cerebus Neural Signal Processor (Blackrock Microsystems) and saved for offline sorting. Extracted spikes were semi-automatically sorted using Plexon Offline Sorter (Plexon Inc.), and then manually sorted by two raters (BWC and MA).

Experimental setup

The animals completed the task while seated in front of a computer monitor (27″ ASUS VG278H monitor, 1024x768 pixel resolution at a 75 Hz refresh rate) and used a two-axis joystick to freely navigate through the virtual environment. They were placed in a radiofrequency shielded dark room, with cables entering the room through a small aperture. The monkeys' head position was fixed during the task, and eye position was recorded using video-oculography at a sampling rate of 500Hz (EyeLink 1000, SR Research). Custom software was used to simultaneously control and record the stimulus presentation, behavioral response, eye position and reward dispense (Figure 1A).

Behavioral tasks

The learning task was completed in an X-shaped maze as previously described.[21,25,44] In each trial, animals start at one end of the X-maze and navigate toward the corridor using a joystick. Once they enter the corridor, the walls change their texture to either a wood or steel texture. As they continue navigating toward the end of the corridor, two different colored discs appear at each end of the X-maze. One wall texture (the context) is associated with one color (e.g., steel means the target is green, and wood means the target is red) indicating the monkeys to navigate to the corresponding disc to obtain a juice reward. The monkey then turns around to navigate back toward the other end of the maze initiating another trial. Figure 1C demonstrates the trajectory of an example trial.

Each day, monkeys completed a set of trials with a fixed context-color combination, which associated the steel context with the orange target, and the wood context with the purple target. Following this fixed combination, two different colors are

pseudo-randomly chosen to be associated with each context. Therefore, the monkeys must learn a new association for each session. For a given trial, the colors can appear in one of two possible configurations, referred to as color pair order (CPO). Figure 1D demonstrates the different possible task elements for each session: context, CPO and target side. For a given trial, the context and CPO are chosen randomly. We only used novel sessions for our single neuron analyses, highlighted in Figure S1C. All novel sessions shown in Figure S1C were used for our population analyses, in addition to 5 fixed sessions for Monkey B and 3 fixed sessions for Monkey T.

QUANTIFICATION AND STATISTICAL ANALYSIS

All quantification and statistical analyses were completed using MATLAB 2020a. Proportions were compared using Fisher's exact tests or Chi-squared tests. Continuous variables were analyzed using Wilcoxon sign rank tests in cases of paired comparisons, and Wilcoxon rank sum tests in cases of unpaired comparisons. Mean values along with standard errors (SE) were presented for continuous variables. Specific details for each statistical test, including the number of observations and what each observation represents, are included in the manuscript text, figure legends, and figures. P-values >0.05 denote non-significance (ns); * *p-value*s <0.05, ** *p-value*s <0.01, and *** *p-value*s <0.001.

Behavioral analysis

For each session, learning was estimated using a state-space analysis based on all completed trials as previously described.[45] A learning state with a 95% confidence interval is estimated across all completed trials, as illustrated in Figures 1E and S1C. Learning of the association is defined as the 2.5th percentile of the learning state's confidence interval exceeding 50%.

Single neuron tuning

Single neuron tuning over task epochs was computed by calculating the mean firing rate (FR) over 400ms windows with 20ms step sizes. Each unit's mean FR was z-scored across all trials. Given a limited number of incorrect trials, only correct trials were used. We fit each neuron's normalized FR to each feature using a multivariable linear regression (Equation 1), with significance to each feature determined by setting an alpha of 0.01.

$$FR = \beta_0 + \beta_1[Context] + \beta_2[CPO] + \beta_3[target\ side] + \epsilon \quad \text{(Equation 1)}$$

A given unit was defined as being tuned to a feature if it remained tuned for at least five consecutive 20ms sliding windows (i.e., across 100ms). In the model context is the wall color (2 values: wood or steel), CPO is color pair order, the color combination order (2 values: color1 left and color2 right and vice versa), and target side is the location of the target in egocentric space (left or right). The total number of tuned units for each time-window were summed for each feature, and proportions of tuned neurons were compared across the dorsal and ventral LPFC using Fisher's exact test. The proportions of neurons tuned at individual time points were compared using Chi-squared tests. The latency for a given unit's tuning was determined as the first time-window it was significantly tuned to a given feature., and a significant proportion of neurons was determined if the total proportion exceeded the alpha threshold set. Individual neuron tuning latencies were compared for different task features using a Wilcoxon rank-sum test.

Given that eye position was unrestrained, we sought to account for the variance of neural activity explained by this feature and control for it. We limited our analysis to −200ms (−600ms to −200ms window) to 1200ms (800ms–1200ms window) around goal onset because eye position was reliably measured during this time. We first performed a two-step multivariable linear regression (Equations 2 and 3), using mean x and y eye positions in the same 400ms windows we used to analyze the neural data. We fit each unit's normalized FR to the mean x and y eye position, and their interaction to account for neural activity specific to a particular position on the screen (Equation 2). We then utilize the residual FR data, representing the neural activity not accounted for by eye position, to fit a second multivariable linear regression with task-dependent features (Equation 3). Finally, we used Equation 4 to investigate for non-linear mixed selectivity between task features and eye position (Eye_y not shown, but included in the model).

$$FR = \beta_0 + \beta_1[Eye_x] + \beta_2[Eye_y] + \beta_3[Eye_x][Eye_y] + FR\epsilon \quad \text{(Equation 2)}$$

$$FR\epsilon = \beta_0 + \beta_1[Context] + \beta_2[CPO] + \beta_3[target\ side] + FR\epsilon_2 \quad \text{(Equation 3)}$$

$$FR\epsilon_2 = \beta_0 + \beta_1[Context][Eye_x] + \beta_2[CPO]\,[Eye_x] + \epsilon \quad \text{(Equation 4)}$$

One session had at least 15 incorrect trials for each condition, allowing us to examine non-linear mixed selectivity (Figure S2C) using the following equation.

$$FR = \beta_0 + \beta_1[Context] + \beta_2[CPO] + \beta_3[target\ side] + \beta_1[Context][CPO] + \epsilon \quad \text{(Equation 5)}$$

Decoding from population neural activity

We used a linear support vector machine (SVM) to decode task-dependent features from neuronal population activity in single trials in 400ms windows. We initially used only correct trials, with four possible conditions. We utilized the fitcsvm function (MATLAB 2020a)

using a 5-fold cross validation on normalized FRs. Sessions were analyzed separately, and only sessions with at least 15 trials per condition were used. For each session, 15 trials for each condition were randomly chosen and stratified into 5-folds with 1-fold used for testing. This procedure was repeated 100 times, with 500 trained classifiers. In individual sessions, significance was determined by permutation testing, with the previous procedure performed on shuffled trials. Trials were shuffled after the k-fold stratification, and this procedure was repeated 100 times, with 500 classifiers. In individual sessions, significance was determined by a mean accuracy exceeding the 97.5th percentile chance accuracy. We performed the above analysis on normalized FRs from sorted neurons and normalized multiunit activity across each channel.

To control for possible biases in eye position that may affect neural activity we sought to quantify the classification accuracy of task-features from eye position. We calculated the mean x and y eye position across the same 400ms windows as previously described. A linear SVM was used to classify task-features from x and y eye position on the same randomly selected and stratified trials used for the neural data. This was repeated 100 times, generating 500 classifiers. Permutation testing as described above was used for significance testing in individual sessions. The mean decoding accuracies (with standard errors) of task features were calculated across sessions. Decoding accuracies were compared across sessions using the dorsal and ventral LPFC's neural data and eye position at three 400ms windows (centered at 0ms 400ms and 800ms) using Wilcoxon sign rank tests.

Cross-temporal decoding analysis

Cross-temporal decoding was performed to investigate whether the neural code underlying task features was persistent or dynamic across the goal onset epoch. We calculated the mean FR across 400ms windows overlapped by 20ms, and randomly selected trials which were stratified in five k-folds. This was performed from −400ms to 1000ms around the goal onset, with 70 separate time-windows. A linear SVM was used to generate a model on 4 k-folds at each time-window and tested on the same remaining k-fold across all 400ms time-windows (70 time windows). This procedure was then repeated 100 times, resulting in 35 000 separate models (70 × 5 × 100). The mean decoding accuracy across sessions (with the standard error) was calculated, and significance was determined when the bottom 2.5th percentile decoding accuracy exceeded chance performance. Cross-temporal decoding analysis was statistically compared across models trained at three time windows (centered at 0ms, 400ms and 800ms) around goal onset using a Wilcoxon sign rank test.

Dimensionality reduction and state-space analysis

We investigated the dimensionality and variance of neural activity explained in six novel sessions from Monkey B, using the same 400ms windows used in previous analyses. We initially performed principal components analysis (PCA) on normalized neural activity at 200ms, 600ms, and 1000ms. The variance explained by the top 30 PCs at each time is shown in Figure S8A. To find an axis in this space that explains eye position, we used a multivariable linear regression with the neural activity projected on the top 30 PCs as independent variables. The coefficients were normalized to provide a unit vector representing the Eye_x axis. We then used neural data projected on the null space of eye position axis as predictors in linear discriminant analysis (LDA) to find axes that represent context and CPO. Neural data was projected on those axes, and the variance of that projected neural activity explained by task features was quantified with a linear regression (Figure S8A).

To visualize neural trajectories over time, we concatenated neural activity across all time points, providing a matrix with rows equal to the number of neurons, and columns equal to the number of trials by the number of time points. Otherwise, we performed the same analysis as above, also using the top 30 PCs. The variance of neural activity explained by task features at each time point using this analysis is shown in Figure S8B. This was compared to the variance explained by performing the analysis described above at each individual time point. Using the temporally concatenated neural activity explained less variance, especially at 200ms and 1000ms (Figure S8B). However, this still captured the overall neural dynamics, particularly at 600ms. Finally, this analysis was cross-validated with one left out trial which was projected on the dimensions identified using the other trials. The Euclidean distance of individual trials and trials averaged across task conditions was compared using Wilcoxon rank-sum test.